Title
Study of inclusive production of charmonium mesons in B decays

Journal
Physical Review D, 67(3)

ISSN
2470-0010

Authors
Aubert, B
Boutigny, D
Gaillard, J-M
et al.

Publication Date
2003-02-01

DOI
10.1103/physrevd.67.032002

Study of inclusive production of charmonium mesons in *B* decays

B. Aubert, D. Boutigny, J.-M. Gaillard, A. Hicheur, Y. Karyotakis, J. P. Lees, P. Robbe, V. Tisserand, and A. Zghiche
Laboratoire de Physique des Particules, F-74941 Annecy-le-Vieux, France

A. Palano and A. Pompili
Università di Bari, Dipartimento di Fisica and INFN, I-70126 Bari, Italy

J. C. Chen, N. D. Qi, G. Rong, P. Wang, and Y. S. Zhu
Institute of High Energy Physics, Beijing 100039, China

G. Eigen, I. Ofte, and B. Stugu
University of Bergen, Institute of Physics, N-5007 Bergen, Norway

G. S. Abrams, A. W. Borgland, A. B. Breon, D. N. Brown, J. Button-Shafer, R. N. Cahn, E. Charles, M. S. Gill, A. V. Gritsan, Y. Groysman, R. G. Jacobsen, R. W. Kadel, J. Kadyk, L. T. Kerth, Yu. G. Kolomensky, J. F. Kral, C. LeClerc, M. E. Levi, G. Lynch, L. M. Mir, P. J. Oddone, T. Orimoto, M. Pripstein, N. A. Roe, A. Romosan, M. T. Ronan, V. G. Shelkov, A. V. Telnov, and W. A. Wenzel
Lawrence Berkeley National Laboratory and University of California, Berkeley, California 94720

T. J. Harrison, C. M. Hawkes, D. J. Knowles, S. W. O'Neale, R. C. Penny, A. T. Watson, and N. K. Watson
University of Birmingham, Birmingham, B15 2TT, United Kingdom

T. Deppermann, K. Goetzen, H. Koch, B. Lewandowski, K. Peters, H. Schmuecker, and M. Steinke
Ruhr Universität Bochum, Institut für Experimentalphysik 1, D-44780 Bochum, Germany

N. R. Barlow, W. Bhimji, J. T. Boyd, N. Chevalier, P. J. Clark, W. N. Cottingham, C. Mackay, and F. F. Wilson
University of Bristol, Bristol BS8 1TL, United Kingdom

K. Abe, C. Hearty, T. S. Mattison, J. A. McKenna, and D. Thiessen
University of British Columbia, Vancouver, British Columbia, Canada V6T 1Z1

S. Jolly and A. K. McKemey
Brunel University, Uxbridge, Middlesex UB8 3PH, United Kingdom

V. E. Blinov, A. D. Bukin, A. R. Buzykaev, V. B. Golubev, V. N. Ivanchenko, A. A. Korol, E. A. Kravchenko, A. P. Onuchin, S. I. Serednyakov, Yu. I. Skovpen, and A. N. Yushkov
Budker Institute of Nuclear Physics, Novosibirsk 630090, Russia

D. Best, M. Chao, D. Kirkby, A. J. Lankford, M. Mandelkern, S. McMahon, and D. P. Stoker
University of California at Irvine, Irvine, California 92697

K. Arisaka, C. Buchanan, and S. Chun
University of California at Los Angeles, Los Angeles, California 90024

D. B. MacFarlane, S. Prell, Sh. Rahatlou, G. Raven, and V. Sharma
University of California at San Diego, La Jolla, California 92093

J. W. Berryhill, C. Campagnari, B. Dahmes, P. A. Hart, N. Kuznetsova, S. L. Levy, O. Long, A. Lu, M. A. Mazur, J. D. Richman, and W. Verkerke
University of California at Santa Barbara, Santa Barbara, California 93106

J. Beringer, A. M. Eisner, M. Grothe, C. A. Heusch, W. S. Lockman, T. Pulliam, T. Schalk, R. E. Schmitz, B. A. Schumm, A. Seiden, M. Turri, W. Walkowiak, D. C. Williams, and M. G. Wilson
University of California at Santa Cruz, Institute for Particle Physics, Santa Cruz, California 95064

E. Chen, G. P. Dubois-Felsmann, A. Dvoretskii, D. G. Hitlin, F. C. Porter, A. Ryd, A. Samuel, and S. Yang
California Institute of Technology, Pasadena, California 91125

S. Jayatilleke, G. Mancinelli, B. T. Meadows, and M. D. Sokoloff
University of Cincinnati, Cincinnati, Ohio 45221

0556-2821/2003/67(3)/032002(14)/$20.00

T. Barillari, P. Bloom, W. T. Ford, U. Nauenberg, A. Olivas, P. Rankin, J. Roy, J. G. Smith, W. C. van Hoek, and L. Zhang
University of Colorado, Boulder, Colorado 80309

J. Blouw, J. L. Harton, M. Krishnamurthy, A. Soffer, W. H. Toki, R. J. Wilson, and J. Zhang
Colorado State University, Fort Collins, Colorado 80523

D. Altenburg, T. Brandt, J. Brose, T. Colberg, M. Dickopp, R. S. Dubitzky, A. Hauke, E. Maly, R. Müller-Pfefferkorn, S. Otto, K. R. Schubert, R. Schwierz, B. Spaan, and L. Wilden
Technische Universität Dresden, Institut für Kern-und Teilchenphysik, D-01062 Dresden, Germany

D. Bernard, G. R. Bonneaud, F. Brochard, J. Cohen-Tanugi, S. Ferrag, S. T'Jampens, Ch. Thiebaux, G. Vasileiadis, and M. Verderi
Ecole Polytechnique, LLR, F-91128 Palaiseau, France

A. Anjomshoaa, R. Bernet, A. Khan, D. Lavin, F. Muheim, S. Playfer, J. E. Swain, and J. Tinslay
University of Edinburgh, Edinburgh EH9 3JZ, United Kingdom

M. Falbo
Elon University, Elon University, North Carolina 27244-2010

C. Borean, C. Bozzi, L. Piemontese, and A. Sarti
Università di Ferrara, Dipartimento di Fisica and INFN, I-44100 Ferrara, Italy

E. Treadwell
Florida A&M University, Tallahassee, Florida 32307

F. Anulli,* R. Baldini-Ferroli, A. Calcaterra, R. de Sangro, D. Falciai, G. Finocchiaro, P. Patteri, I. M. Peruzzi,* M. Piccolo, and A. Zallo
Laboratori Nazionali di Frascati dell'INFN, I-00044 Frascati, Italy

S. Bagnasco, A. Buzzo, R. Contri, G. Crosetti, M. Lo Vetere, M. Macri, M. R. Monge, S. Passaggio, F. C. Pastore, C. Patrignani, E. Robutti, A. Santroni, and S. Tosi
Università di Genova, Dipartimento di Fisica and INFN, I-16146 Genova, Italy

M. Morii
Harvard University, Cambridge, Massachusetts 02138

R. Bartoldus, G. J. Grenier, and U. Mallik
University of Iowa, Iowa City, Iowa 52242

J. Cochran, H. B. Crawley, J. Lamsa, W. T. Meyer, E. I. Rosenberg, and J. Yi
Iowa State University, Ames, Iowa 50011-3160

M. Davier, A. Höcker, H. M. Lacker, S. Laplace, F. Le Diberder, G. Grosdidier, V. Lepeltier, A. M. Lutz, T. C. Petersen, S. Plaszczynski, M. H. Schune, L. Tantot, S. Trincaz-Duvoid, and G. Wormser
Laboratoire de l'Accélérateur Linéaire, F-91898 Orsay, France

R. M. Bionta, V. Brigljević, D. J. Lange, M. Mugge, K. van Bibber, and D. M. Wright
Lawrence Livermore National Laboratory, Livermore, California 94550

A. J. Bevan, J. R. Fry, E. Gabathuler, R. Gamet, M. George, M. Kay, D. J. Payne, R. J. Sloane, and C. Touramanis
University of Liverpool, Liverpool L69 3BX, United Kingdom

M. L. Aspinwall, D. A. Bowerman, P. D. Dauncey, U. Egede, I. Eschrich, G. W. Morton, J. A. Nash, P. Sanders, D. Smith, and G. P. Taylor
University of London, Imperial College, London, SW7 2BW, United Kingdom

J. J. Back, G. Bellodi, P. Dixon, P. F. Harrison, R. J. L. Potter, H. W. Shorthouse, P. Strother, and P. B. Vidal
Queen Mary, University of London, E1 4NS, United Kingdom

G. Cowan, H. U. Flaecher, S. George, M. G. Green, A. Kurup, C. E. Marker, T. R. McMahon, S. Ricciardi, F. Salvatore, G. Vaitsas, and M. A. Winter
University of London, Royal Holloway and Bedford New College, Egham, Surrey TW20 0EX, United Kingdom

D. Brown and C. L. Davis
University of Louisville, Louisville, Kentucky 40292

J. Allison, R. J. Barlow, A. C. Forti, F. Jackson, G. D. Lafferty, N. Savvas, J. H. Weatherall, and J. C. Williams
University of Manchester, Manchester M13 9PL, United Kingdom

A. Farbin, A. Jawahery, V. Lillard, D. A. Roberts, and J. R. Schieck
University of Maryland, College Park, Maryland 20742

G. Blaylock, C. Dallapiccola, K. T. Flood, S. S. Hertzbach, R. Kofler, V. B. Koptchev, T. B. Moore, H. Staengle, and S. Willocq
University of Massachusetts, Amherst, Massachusetts 01003

B. Brau, R. Cowan, G. Sciolla, F. Taylor, and R. K. Yamamoto
Massachusetts Institute of Technology, Laboratory for Nuclear Science, Cambridge, Massachusetts 02139

M. Milek and P. M. Patel
McGill University, Montréal, QC, Canada H3A 2T8

F. Palombo
Università di Milano, Dipartimento di Fisica and INFN, I-20133 Milano, Italy

J. M. Bauer, L. Cremaldi, V. Eschenburg, R. Kroeger, J. Reidy, D. A. Sanders, and D. J. Summers
University of Mississippi, University, Mississippi 38677

C. Hast and P. Taras
Université de Montréal, Laboratoire René J. A. Lévesque, Montréal, QC, Canada H3C 3J7

H. Nicholson
Mount Holyoke College, South Hadley, Massachusetts 01075

C. Cartaro, N. Cavallo, G. De Nardo, F. Fabozzi, C. Gatto, L. Lista, P. Paolucci, D. Piccolo, and C. Sciacca
Università di Napoli Federico II, Dipartimento di Scienze Fisiche and INFN, I-80126, Napoli, Italy

J. M. LoSecco
University of Notre Dame, Notre Dame, Indiana 46556

J. R. G. Alsmiller and T. A. Gabriel
Oak Ridge National Laboratory, Oak Ridge, Tennessee 37831

J. Brau, R. Frey, M. Iwasaki, C. T. Potter, N. B. Sinev, D. Strom, and E. Torrence
University of Oregon, Eugene, Oregon 97403

F. Colecchia, A. Dorigo, F. Galeazzi, M. Margoni, M. Morandin, M. Posocco, M. Rotondo, F. Simonetto, R. Stroili, and C. Voci
Università di Padova, Dipartimento di Fisica and INFN, I-35131 Padova, Italy

M. Benayoun, H. Briand, J. Chauveau, P. David, Ch. de la Vaissière, L. Del Buono, O. Hamon, Ph. Leruste, J. Ocariz, M. Pivk, L. Roos, and J. Stark
Universités Paris VI et VII, Lab de Physique Nucléaire H. E., F-75252 Paris, France

P. F. Manfredi, V. Re, and V. Speziali
Università di Pavia, Dipartimento di Elettronica and INFN, I-27100 Pavia, Italy

L. Gladney, Q. H. Guo, and J. Panetta
University of Pennsylvania, Philadelphia, Pennsylvania 19104

C. Angelini, G. Batignani, S. Bettarini, M. Bondioli, F. Bucci, G. Calderini, E. Campagna, M. Carpinelli, F. Forti, M. A. Giorgi, A. Lusiani, G. Marchiori, F. Martinez-Vidal, M. Morganti, N. Neri, E. Paoloni, M. Rama, G. Rizzo, F. Sandrelli, G. Triggiani, and J. Walsh
Università di Pisa, Scuola Normale Superiore and INFN, I-56010 Pisa, Italy

M. Haire, D. Judd, K. Paick, L. Turnbull, and D. E. Wagoner
Prairie View A&M University, Prairie View, Texas 77446

J. Albert, P. Elmer, C. Lu, V. Miftakov, J. Olsen, S. F. Schaffner, A. J. S. Smith, A. Tumanov, and E. W. Varnes
Princeton University, Princeton, New Jersey 08544

F. Bellini, G. Cavoto, D. del Re, F. Ferrarotto, F. Ferroni, E. Leonardi, M. A. Mazzoni, S. Morganti, G. Piredda, F. Safai Tehrani, M. Serra, and C. Voena
Università di Roma La Sapienza, Dipartimento di Fisica and INFN, I-00185 Roma, Italy

R. Faccini
University of California at San Diego, La Jolla, California 92093
and Università di Roma La Sapienza, Dipartimento di Fisica and INFN, I-00185 Roma, Italy

S. Christ, G. Wagner, and R. Waldi
Universität Rostock, D-18051 Rostock, Germany

T. Adye, N. De Groot, B. Franek, N. I. Geddes, G. P. Gopal, and S. M. Xella
Rutherford Appleton Laboratory, Chilton, Didcot, Oxon, OX11 0QX, United Kingdom

R. Aleksan, S. Emery, A. Gaidot, P.-F. Giraud, G. Hamel de Monchenault, W. Kozanecki, M. Langer, G. W. London, B. Mayer, G. Schott, B. Serfass, G. Vasseur, Ch. Yeche, and M. Zito
DAPNIA, Commissariat à l'Energie Atomique/Saclay, F-91191 Gif-sur-Yvette, France

M. V. Purohit, A. W. Weidemann, and F. X. Yumiceva
University of South Carolina, Columbia, South Carolina 29208

I. Adam, D. Aston, N. Berger, A. M. Boyarski, M. R. Convery, D. P. Coupal, D. Dong, J. Dorfan, W. Dunwoodie, R. C. Field, T. Glanzman, S. J. Gowdy, E. Grauges, T. Haas, T. Hadig, V. Halyo, T. Himel, T. Hryn'ova, M. E. Huffer, W. R. Innes, C. P. Jessop, M. H. Kelsey, P. Kim, M. L. Kocian, U. Langenegger, D. W. G. S. Leith, S. Luitz, V. Luth, H. L. Lynch, H. Marsiske, S. Menke, R. Messner, D. R. Muller, C. P. O'Grady, V. E. Ozcan, A. Perazzo, M. Perl, S. Petrak, H. Quinn, B. N. Ratcliff, S. H. Robertson, A. Roodman, A. A. Salnikov, T. Schietinger, R. H. Schindler, J. Schwiening, G. Simi, A. Snyder, A. Soha, S. M. Spanier, J. Stelzer, D. Su, M. K. Sullivan, H. A. Tanaka, J. Va'vra, S. R. Wagner, M. Weaver, A. J. R. Weinstein, W. J. Wisniewski, D. H. Wright, and C. C. Young
Stanford Linear Accelerator Center, Stanford, California 94309

P. R. Burchat, C. H. Cheng, T. I. Meyer, and C. Roat
Stanford University, Stanford, California 94305-4060

R. Henderson
TRIUMF, Vancouver, British Columbia, Canada V6T 2A3

W. Bugg and H. Cohn
University of Tennessee, Knoxville, Tennessee 37996

J. M. Izen, I. Kitayama, and X. C. Lou
University of Texas at Dallas, Richardson, Texas 75083

F. Bianchi, M. Bona, and D. Gamba
Università di Torino, Dipartimento di Fisica Sperimentale and INFN, I-10125 Torino, Italy

L. Bosisio, G. Della Ricca, S. Dittongo, L. Lanceri, P. Poropat, L. Vitale, and G. Vuagnin
Università di Trieste, Dipartimento di Fisica and INFN, I-34127 Trieste, Italy

R. S. Panvini
Vanderbilt University, Nashville, Tennessee 37235

S. W. Banerjee, C. M. Brown, D. Fortin, P. D. Jackson, R. Kowalewski, and J. M. Roney
University of Victoria, Victoria, British Columbia, Canada V8W 3P6

H. R. Band, S. Dasu, M. Datta, A. M. Eichenbaum, H. Hu, J. R. Johnson, R. Liu, F. Di Lodovico, Y. Pan, R. Prepost, I. J. Scott, S. J. Sekula, J. H. von Wimmersperg-Toeller, J. Wu, S. L. Wu, and Z. Yu
University of Wisconsin, Madison, Wisconsin 53706

H. Neal
Yale University, New Haven, Connecticut 06511

(*BABAR* Collaboration)
(Received 29 July 2002; published 27 February 2003)

The inclusive production of charmonium mesons in B meson decay has been studied in a 20.3 fb^{-1} data set collected by the *BABAR* experiment operating at the $\Upsilon(4S)$ resonance. Branching fractions have been measured for the inclusive production of the charmonium mesons J/ψ, $\psi(2S)$, χ_{c1}, and χ_{c2}. The branching fractions are also presented as a function of the center-of-mass momentum of the mesons and of the helicity of the J/ψ.

DOI: 10.1103/PhysRevD.67.032002 PACS number(s): 13.25.Hw, 14.40.Gx

I. INTRODUCTION

Studies of the inclusive production of charmonium mesons in B decays provide insight into the physics of the underlying production mechanisms. Nonrelativistic QCD (NRQCD) [1], which may provide an explanation [2] for the unexpectedly large production of J/ψ and $\psi(2S)$ mesons observed in $p\bar{p}$ collisions [3], is an example of such a mechanism. NRQCD calculations use phenomenological matrix elements that should be applicable to a variety of production processes [4], including such kinematically different regimes as hadron collisions at the Fermilab Tevatron collider and e^+e^- collisions at the $\Upsilon(4S)$.

This paper presents an analysis of J/ψ, χ_{c1}, χ_{c2}, and $\psi(2S)$ mesons produced in B decays at the $\Upsilon(4S)$ resonance. J/ψ and $\psi(2S)$ mesons are reconstructed in the e^+e^- and $\mu^+\mu^-$ decay modes, and the χ_{c1} and χ_{c2} in the $J/\psi\gamma$ final states. We also reconstruct $\psi(2S)\to J/\psi\pi^+\pi^-$.

The results include new measurements of previously observed decays [5,6] as well as momentum and helicity distributions not previously measured.

II. THE *BABAR* DETECTOR AND THE PEP-II COLLIDER

The *BABAR* detector is located at the PEP-II e^+e^- storage rings operating at the Stanford Linear Accelerator Center. At PEP-II, 9.0 GeV electrons collide with 3.1 GeV positrons to produce a center-of-mass energy of 10.58 GeV, the mass of the $\Upsilon(4S)$ resonance.

The *BABAR* detector is described elsewhere [7]; here we give only a brief overview. Surrounding the interaction point is a 5-layer double-sided silicon vertex tracker (SVT), which provides precision spatial information for all charged particles, and also measures their energy loss (dE/dx). The SVT is the primary detection device for low momentum charged particles. Outside the SVT, a 40-layer drift chamber (DCH) provides measurements of the transverse momenta p_T of charged particles with respect to the beam direction. The resolution of the p_T measurement for tracks with momenta above 1 GeV/c is parametrized as

$$\frac{\sigma(p_T)}{p_T} = 0.13 \cdot p_T\% + 0.45\%, \tag{1}$$

where p_T is measured in GeV/c. The drift chamber also measures dE/dx with a resolution of 7.5%. Beyond the outer radius of the DCH is a detector of internally reflected Cherenkov radiation (DIRC), which is used primarily for charged hadron identification. The detector consists of quartz bars in which Cherenkov light is produced as relativistic charged particles traverse the material. The light is internally reflected along the length of the bar into a water-filled stand-off box mounted on the rear of the detector. The Cherenkov rings expand in the stand-off box and are measured with an array of photomultiplier tubes mounted on its outer surface. A CsI(Tl) crystal electromagnetic calorimeter (EMC) is used to detect photons and neutral hadrons, as well as to identify electrons. The energy resolution of the calorimeter is parametrized as

$$\frac{\sigma(E)}{E} = \frac{2.3\%}{E^{1/4}} \oplus 1.9\%, \tag{2}$$

where the energy E is measured in GeV. The EMC is surrounded by a superconducting solenoid that produces a 1.5-T magnetic field. The instrumented flux return (IFR) consists of multiple layers of resistive plate chambers (RPC) interleaved with the flux return iron. The IFR is used in the identification of muons and neutral hadrons.

*Also with Università di Perugia, I-06100 Perugia, Italy.

Data acquisition is triggered with a two-level system. The first level uses fast algorithms implemented in hardware that examine tracks in the DCH and energetic clusters in the EMC. The second level retains events in which the track candidates point back to the beam interaction region, or in which the EMC cluster candidates are correlated in time with the rest of the event and exceed the energy of a minimum ionizing particle. Over 99.9% of $B\overline{B}$ events pass the second level trigger. A fraction of all events that pass the first level are passed through the second to allow monitoring of its performance.

III. COORDINATE SYSTEM AND REFERENCE FRAMES

We use a right-handed coordinate system with the z axis along the electron beam direction and the y axis upwards, with origin at the nominal beam interaction point. The polar angle θ is measured from the z axis and the azimuthal angle ϕ from the x axis. Unless otherwise stated, kinematic quantities are calculated in the rest frame of the detector. The other reference frame we commonly use is the center of mass of the colliding electrons and positrons, which we call the center-of-mass frame.

IV. EVENT SELECTION

The data used in these analyses were collected between October 1999 and October 2000 and correspond to an integrated luminosity of 20.3 fb^{-1} taken on the $\Upsilon(4S)$ and 2.6 fb^{-1} taken off-resonance at an energy 0.04 GeV lower than the peak, which is below the threshold for $B\overline{B}$ production and therefore includes only continuum processes.

We use an equivalent luminosity of simulated data [8], including both $B\overline{B}$ and continuum, to study the efficiency of the analysis.

We require events to satisfy criteria that are intended to have high efficiency for $\Upsilon(4S)$ events while rejecting a significant fraction of continuum events and strongly suppressing beam gas events. The event must satisfy either the DCH components of both trigger levels or the EMC components of both, and have three or more high-quality tracks in the angular region with full tracking acceptance, $0.41<\theta<2.54$. Reconstructed charged particles are considered high-quality tracks if they have at least 12 hits in the DCH, $p_T>100\ \mathrm{MeV}/c$, and a point of closest approach to the beam spot of <3 cm in z and <1.5 cm in xy.

The ratio of the second to the zeroth Fox-Wolfram moment R_2 [9] measures how uniformly the energy in the event is distributed, distinguishing the more spherical $B\overline{B}$ events with small R_2 from the more jet-like continuum events at large R_2 (Fig. 1). We require $R_2<0.5$.

The primary event vertex is obtained from all charged particles with $0.41<\theta<2.54$. Particles contributing a large χ^2 are removed from the vertex and the process is iterated until stable. To reject events due to a beam particle striking the beam pipe or a residual gas molecule, we require the primary event vertex to be within 0.5 cm of the beam spot in xy and 6 cm in z.

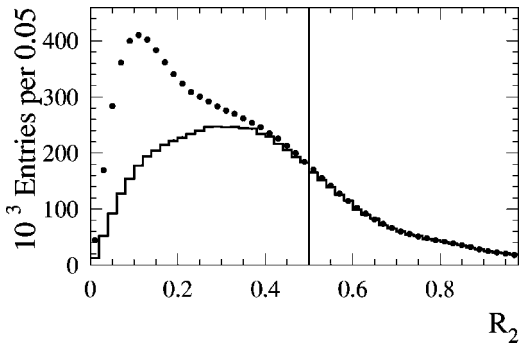

FIG. 1. R_2 distribution after all other selection criteria have been applied. Points are on-resonance data; histogram is off-resonance data scaled to the same luminosity. The vertical line denotes the requirement imposed on R_2.

Finally, the event must include total visible energy (charged particles plus unassociated EMC clusters above 30 MeV) greater than 4.5 GeV.

The efficiency for simulated $\Upsilon(4S)\to B\overline{B}$ events is 95.4%. More relevant is the ratio C_E of this efficiency to that for events containing the charmonium decay of interest. C_E is calculated for each of the final states using simulated data. Inaccuracies in the simulation of the tracking systems produce an uncertainty of 1.1%, common to all modes.

Determination of number of $\Upsilon(4S)$ mesons

The number of $\Upsilon(4S)$ events satisfying the above selection criteria (N_Υ) is obtained from the total number of events satisfying the criteria by subtracting the component due to the continuum.

$$N_\Upsilon = N_{on} - \kappa \cdot R_{off} \cdot M_{on}, \tag{3}$$

where

N_{on} is the number of events satisfying the criteria in the on-resonance data set;
M_{on} is the number of muon pairs in the on-resonance data set;
$R_{off}=N_{off}/M_{off}$ is the ratio of the number of events satisfying the hadronic selection criteria to the number of muon pairs in the off resonance data; and
$\kappa=1.0000\pm0.0025$ allows for differences in the ratios of continuum and muon-pair cross sections and efficiencies between on-resonance and off-resonance data.

The two highest-momentum tracks in muon pair events must both deposit less than 1 GeV in the EMC and satisfy $|\cos\theta|<0.7485$ in the center-of-mass frame (to be within the region of full tracking efficiency). The tracks must be within 10° of being back-to-back, and must have a combined mass greater than 7.5 GeV/c^2. Since the number of muon pairs in the on and off resonance data sets appears only as a ratio in Eq. (3), N_Υ depends only weakly on the details of the selection criteria. Varying these over reasonable ranges changes

N_{Υ} by 0.5%, which we take as a systematic error. The on-resonance data contains 7.8 times as many muon pairs as the off-resonance data.

Changes to the trigger configuration caused R_{off} to vary from 4.89 to 4.94 during the period in which the data was collected. For the purposes of this calculation, the data is grouped into periods of compatible R_{off}. Combining the data in a single group changes N_{Υ} by 0.3%, which is taken as a systematic error. In principle, R_{off} could also vary due to beam gas backgrounds. However, the z distribution of the primary event vertex indicates that less than 0.1% of events are due to beam gas.

We find $N_{\Upsilon}=(21.26\pm0.17)\times10^6$. The 0.8% uncertainty is systematic and includes the 0.5%, 0.3% and 0.1% contributions from muon pairs, R_{off}, and beam gas described above. The largest component is from the 0.25% uncertainty on κ, which corresponds to a 0.6% uncertainty on N_{Υ}.

V. J/ψ PRODUCTION

A. J/ψ reconstruction

We reconstruct J/ψ candidates in selected events using the e^+e^- and $\mu^+\mu^-$ final states. The leptons are required to satisfy the track quality criteria listed earlier. Electron candidates are further required to have a distance of closest approach to the beam line of less than 0.25 cm to reject electrons produced by photon conversions.

Both leptons are required to fall in the angular range $0.410<\theta<2.409$ rad (the overlap of the SVT and EMC coverage). Simulation indicates that $(75.3\pm0.9)\%$ of J/ψ decays give both leptons in this region. As described in Sec. IX A, the J/ψ momentum distribution in the simulation [10] is slightly different from the observed distribution. This difference, and a small variation of efficiency with momentum, produce the uncertainty in the efficiency.

We obtain the efficiency for the leptons to satisfy the quality criteria by comparing the performance of the independent SVT and DCH tracking systems in hadronic events. The corresponding uncertainty in the efficiency is 2.4% per J/ψ.

One particle in a $J/\psi\to e^+e^-$ candidate must satisfy the ''very tight'' electron identification criteria described below. The other must satisfy the ''tight'' criteria displayed in square brackets.

(1) Difference between measured and expected energy loss in the DCH between -2σ and $+4\sigma$, where σ is the measurement error [-3σ and $+7\sigma$];

(2) Ratio of energy measured in EMC to measured momentum E/p in range 0.89 to 1.2 [0.75 to 1.3];

(3) Associated EMC cluster must include at least four crystals [same];

(4) Lateral energy distribution LAT [11] of EMC cluster in range 0.1–0.6 [0.0–0.6];

(5) The A_{42} Zernike moment [12] of the EMC cluster <0.42 [no requirement]; and

(6) DIRC Cherenkov angle within 3σ of expected value [no requirement].

LAT is a measure of the radial energy profile of the cluster, and is used to suppress clusters from electronic noise (very low LAT) or hadronic interactions (high LAT). A_{42} measures the azimuthal asymmetry of the cluster about its peak, distinguishing electromagnetic from hadronic showers.

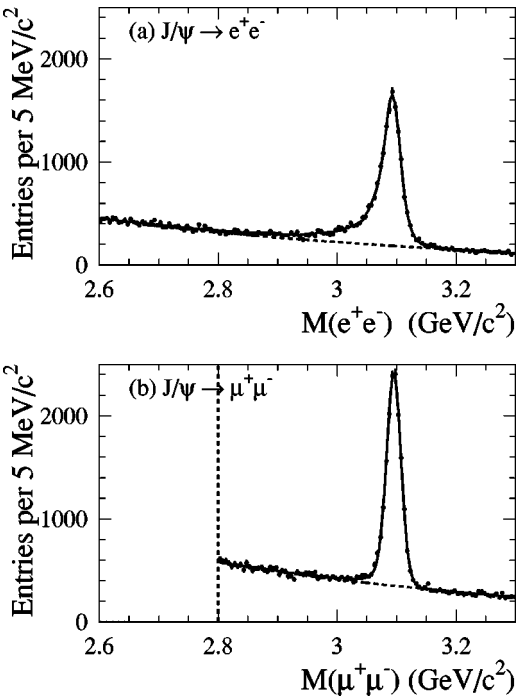

FIG. 2. Mass distribution of J/ψ candidates reconstructed in the (a) e^+e^- and (b) $\mu^+\mu^-$ final states. The vertical dashed line in (b) marks the lower edge of the mass range used in the $\mu^+\mu^-$ final state.

We reduce the impact of bremsstrahlung by combining photons radiated by electron candidates with the track measured in the tracking system (''bremsstrahlung-recovery''). Such photons must have EMC energy greater than 30 MeV and a polar angle within 35 mrad of the electron direction. The azimuthal angle of the photon must be within 50 mrad of the electron direction at the beamspot or be between this direction and azimuthal location of the electron shower in the EMC.

For $J/\psi\to\mu^+\mu^-$ candidates, one muon candidate must satisfy ''tight'' criteria, while the other satisfies ''loose'' criteria (shown in square brackets):

(1) Energy in calorimeter between 0.05 and 0.40 GeV [<0.50 GeV];

(2) Number of IFR layers $N_{IFR}\geqslant2$ [same];

(3) Particle penetrates at least 2.2 interaction lengths λ of detector material [2λ]; (4)

(4) Measured penetration within $\pm0.8\lambda$ of the value expected for that momentum [$\pm1.0\lambda$];

(5) An average of less than 8 hit strips per IFR layer [same];

(6) The RMS of the hits per IFR layer less than 4 [same];

(7) For candidates in the forward endcap, the number of hit IFR layers divided by the total number of layers between the first and last hit layers must be >0.34 to reject beam background in the outermost layer [>0.30];

(8) χ^2 of the track fit in the IFR$<3\times N_{IFR}$ [same]; and

(9) χ^2 of match between track from SVT and DCH and that found in the IFR$<5\times N_{IFR}$ [same].

TABLE I. Meson yield in on-resonance (20.3 fb^{-1}) and off-resonance (2.6 fb^{-1}) data, and net yield after continuum subtraction. ϵ_C and C_E are the meson reconstruction efficiency and the relative event selection efficiency; S_N and S_ϵ are the systematic errors on the meson yield and reconstruction efficiency; *Stat* is the statistical error. The systematic errors on the branching fraction products include components unique to that final state. The total uncertainty values include those listed in the ''Common'' rows. $\mathcal{B}_c$ are the secondary branching fractions and S_B the uncertainty. *Tot* is the total systematic error (percentage) on the *B* branching fraction to that final state.

	Meson Yield N_ψ			Efficiencies		Uncertainties (%)			$\mathcal{B}$ Product$\times 10^6$					
Mode	*On*	*Off*	*Net*	ϵ_C	C_E	S_N	S_ϵ	*Stat*	*Value*	*Stat*	*Sys*	$\mathcal{B}_c$	S_B %	*Tot* %
$J/\psi\to\ell^+\ell^-$														
e^+e^-	16095±242	23±15	15914±268	0.589	1.02	4.1	2.0	1.7	650	±11	±30	0.0593	1.7	4.9
$\mu^+\mu^-$	13683±154	67±18	13159±210	0.500	0.99	0.7	1.4	1.6	615	±10	±10	0.0588	1.7	2.3
Common	-	-	-	-	-	-	3.1	-	-	-	3.1%	-	0.	3.1
$\chi_{c1}\to J/\psi\gamma$														
$J/\psi\to e^+e^-$	512±62	−2±3	528±67	0.191	1.04	6.4	3.1	12.7	68	±9	±5	0.0593	1.7	7.3
$J/\psi\to\mu^+\mu^-$	614±72	3±6	592±86	0.201	1.00	5.4	2.0	14.5	69	±10	±4	0.0588	1.7	6.0
Common	-	-	-	-	-	-	4.5	-	-	-	4.5%	0.316	10.1	11.1
$\chi_{c2}\to J/\psi\gamma$														
$J/\psi\to e^+e^-$	168±48	−5±3	210±54	0.197	1.04	3.9	9.6	25.7	26	±7	±3	0.0593	1.7	10.3
$J/\psi\to\mu^+\mu^-$	208±54	4±5	174±66	0.207	1.00	10.4	12.1	38.0	20	±8	±3	0.0588	1.7	16.0
Common	-	-	-	-	-	-	5.3	-	-	-	5.3%	0.187	10.7	11.9
$\psi(2S)\to\ell^+\ell^-$														
e^+e^-	573±52	−6±8	623±81	0.594	1.05	4.3	1.9	12.9	25.8	±3.3	±1.2	0.0078	-	-
$\mu^+\mu^-$	437±44	5±10	400±92	0.535	1.01	3.1	1.6	23.0	17.8	±4.1	±0.5	0.0067	-	-
Common	-	-	-	-	-	-	3.1	-	-	-	3.1%	-	-	3.1
$\psi(2S)\to J/\psi\pi^+\pi^-$														
$J/\psi\to e^+e^-$	474±43	0±2	476±45	0.205	0.99	2.7	2.1	9.5	53.9	±5.1	±1.8	0.0593	1.7	3.8
$J/\psi\to\mu^+\mu^-$	493±42	0±3	496±47	0.215	0.98	2.3	1.4	9.5	53.3	±5.1	±1.4	0.0588	1.7	3.2
Common	-	-	-	-	-	-	3.5	-	-	-	3.5%	0.305	5.2	6.3

The particle identification efficiencies are obtained by comparing the yield of J/ψ mesons applying various criteria to one or both tracks. The efficiency for $J/\psi\to e^+e^-$ satisfying the angular acceptance and track quality criteria is 90.5% with a systematic error of 1.8%. For $J/\psi\to\mu^+\mu^-$, it is 71.7% with a systematic error of 1.4%. The systematic errors are somewhat conservative, in that they include a component due to the J/ψ statistics. Misidentification of hadrons as muons is higher than misidentification as electrons, producing J/ψ background levels that are approximately a factor of two higher.

Finally, the J/ψ candidate must have momentum in the center of mass $p^*<2.0\ \mathrm{GeV}/c$. This requirement is fully efficient for a J/ψ meson from *B* decay but rejects approximately 74% of those produced in the continuum [13].

More than one J/ψ candidate may be found in an event. A second candidate is observed in 0.8% of events that include at least one.

B. Extraction of number of J/ψ mesons

The mass of the J/ψ candidate is obtained after constraining the two leptons to a common vertex. In less than 1% of events, the vertex fit does not converge, and we instead use four-vector addition to obtain the candidate mass. The mass resolution is poorer by approximately 1% for these events. Figure 2 shows the mass distribution of the selected candidates in the two lepton modes.

The number of J/ψ mesons in the mass window used in the fit (2.6–3.3 GeV/c^2 for the e^+e^- mode, 2.8–3.3 GeV/c^2 for $\mu^+\mu^-$) is determined by a binned likelihood fit to the distribution. The background is represented by a third-order Chebychev polynomial. The probability distribution function (pdf) for the $\mu^+\mu^-$ signal is the distribution from simulation convolved with a Gaussian distribution, with mean (allowing for a systematic shift between simulation and data) and width (allowing for poorer resolution) free to float in the fit. The additional smearing is required because the simulation underestimates the actual amount of material in the detector. The fit returns an offset of 3 MeV/c^2 and an additional resolution of 7.8 MeV/c^2. The total mass resolution in data is approximately 12 MeV/c^2. The simulation includes final state radiation [14] and predicts that (2.7±0.1)% of reconstructed $J/\psi\to\mu^+\mu^-$ candidates fall outside the mass range used in the fit.

To include the impact of bremsstrahlung, the $J/\psi\to e^+e^-$ signal pdf includes four components, corresponding to mesons where neither electron has undergone bremsstrahlung or at least one, and mesons for which the bremsstrahlung-recovery process has located a photon or not. The shapes are derived from simulated data, but the relative weights of three of the four components are allowed to float in the fit. The fraction of events that did not undergo bremsstrahlung but had a photon assigned by the bremsstrahlung-recovery process is nominally fixed to the value predicted by

TABLE II. Summary of B branching fractions (percent) to charmonium mesons with statistical and systematic uncertainties. The direct branching fraction is also listed, where appropriate. The last column contains the world average values [15].

Meson	*Value*	*Stat*	*Sys*	*World Average*
J/ψ	1.057	± 0.012	± 0.040	1.15 ± 0.06
J/ψ direct	0.740	± 0.023	± 0.043	0.80 ± 0.08
χ_{c1}	0.367	± 0.035	± 0.044	0.36 ± 0.05
χ_{c1} direct	0.341	± 0.035	± 0.042	0.33 ± 0.05
χ_{c2}	0.210	± 0.045	± 0.031	0.07 ± 0.04
χ_{c2} direct	0.190	± 0.045	± 0.029	-
$\psi(2S)$	0.297	± 0.020	± 0.020	0.35 ± 0.05

simulation, although it is varied to obtain a systematic error.

An estimated $(7.3 \pm 0.8)\%$ of reconstructed $J/\psi \to e^+e^-$ candidates fall outside the mass range, which can be compared to the value of 6.1% if the relative pdf weights are fixed to the values predicted by simulation.

We perform similar fits to the off-resonance data with all signal fit parameters fixed except for the number of mesons. The result is scaled by the ratio of on- to off-peak luminosity and subtracted to obtain the number of mesons attributable to B decay, which appears in Table I as the net meson yield.

The fitting procedure is validated and systematic errors on its results are obtained by comparing the generated number of events with the fit number of events for many simulated mass distributions convolved with a Gaussian distribution. For the purposes of this test, we increase the statistics of the simulated data by relaxing the particle identification and track-quality requirements. We also test second and fourth-order Chebychev polynomials for the background pdf. We perform these tests for the χ_{c1}, χ_{c2}, and $\psi(2S)$ mass distributions as well.

We vary fit parameters that are fixed during the fit to obtain an additional systematic contribution. In the case of the J/ψ, we vary the bremsstrahlung-recovery error rate from one-half to twice its nominal value. The systematic errors on the fit yields are 0.7% for $J/\psi \to \mu^+\mu^-$ and 4.1% for $J/\psi \to e^+e^-$.

C. Determination of the $B \to J/\psi X$ branching fraction

We calculate values for the $B \to J/\psi X$ branching fraction using the e^+e^- and $\mu^+\mu^-$ final states separately, then combine the two. The equation for the branching fraction is the same for both cases (and for the other mesons studied):

$$\mathcal{B} = \frac{N_\psi}{2 \cdot N_\Upsilon \cdot \epsilon_C \cdot \mathcal{B}_c} \cdot C_E, \tag{4}$$

where

N_ψ is the net number of mesons in the mass fit range after continuum subtraction;

ϵ_C is the efficiency for a meson to satisfy the selection criteria, including the requirement that the mass fall in the mass fit range;

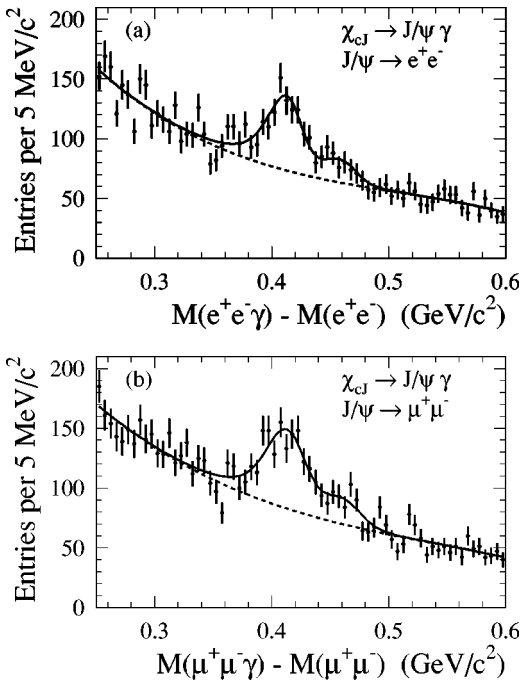

FIG. 3. χ_{c1} and χ_{c2} candidates reconstructed in the $J/\psi\gamma$ final state. Mass difference between the $J/\psi\gamma$ and J/ψ candidates when the J/ψ is reconstructed in the (a) e^+e^- and (b) $\mu^+\mu^-$ final states.

$\mathcal{B}_c$ is world average [15] for the relevant secondary charmonium branching fraction. For the J/ψ, this is for $J/\psi \to e^+e^-$ or $J/\psi \to \mu^+\mu^-$;

C_E corrects for the difference in event selection efficiency (Sec. IV) between generic $B\overline{B}$ events and charmonium events. It is equal to the efficiency for generic $B\overline{B}$ events divided by the efficiency for the relevant charmonium final state.

Table I summarizes the meson yields and efficiencies. It also presents the branching fraction product $\mathcal{B} \cdot \mathcal{B}_c$, an experimental quantity that does not depend on the secondary charmonium branching fractions. There is a 3.1% systematic error common to both modes—and, in fact, to all final states we study—due to acceptance (1.2%), track quality selection (2.4%), uncertainty on C_E (1.1%), and number of $\Upsilon(4S)$ (0.8%).

The separate e^+e^- and $\mu^+\mu^-$ branching fraction measurements are averaged to obtain the final result (Table II). Each measurement is weighted in the average by the inverse of the square of the statistical error plus the square of the systematic errors unique to that mode. The common systematic error is the largest component of the $\mathcal{B}(B \to J/\psi X)$ uncertainty.

VI. χ_c PRODUCTION

We reconstruct χ_{c1} and χ_{c2} mesons in the $J/\psi\gamma$ decay mode. The J/ψ mesons must satisfy the criteria listed in Sec. V A, with the additional requirement that the J/ψ candidate mass m satisfy $3.05 < m < 3.12$ GeV/c^2 for e^+e^- decays and $3.07 < m < 3.12$ GeV/c^2 for $\mu^+\mu^-$. An estimated (74.0

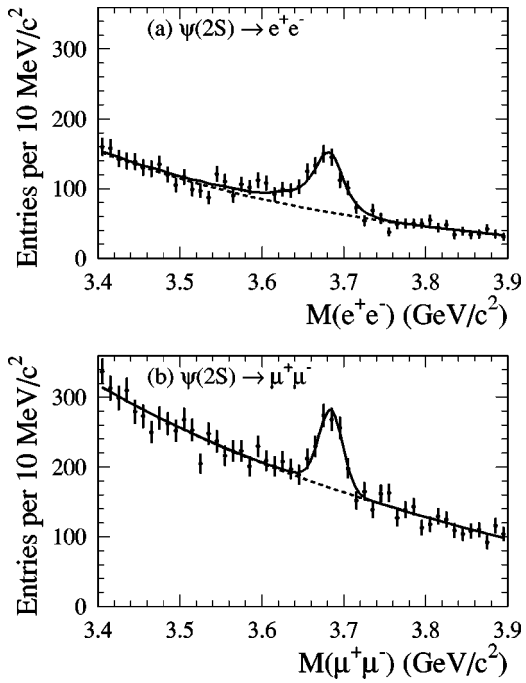

FIG. 4. Mass distribution of $\psi(2S)$ candidates reconstructed in the (a) e^+e^- and (b) $\mu^+\mu^-$ final states.

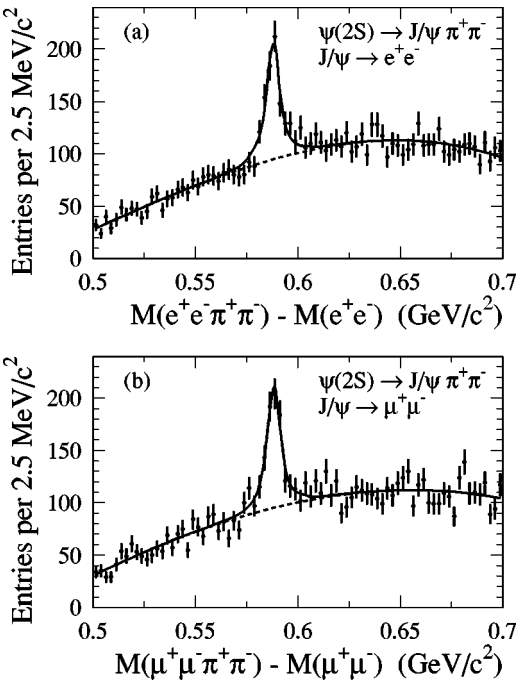

FIG. 5. $\psi(2S)$ candidates reconstructed in the $J/\psi\pi^+\pi^-$ final state. Mass difference between the $J/\psi\pi^+\pi^-$ and J/ψ candidates when the J/ψ is reconstructed in the (a) e^+e^- and (b) $\mu^+\mu^-$ final states.

$\pm 0.4)\%$ of $J/\psi\to e^+e^-$ and $(91.4\pm 0.3)\%$ of $J/\psi \to\mu^+\mu^-$ mesons that satisfy all other criteria satisfy this additional mass selection.

Photon candidates are EMC clusters in the angular range $0.41<\theta<2.409$ rad with energy between 0.12 GeV and 1.0 GeV. Hadronic showers are suppressed by requiring LAT less than 0.8 and $A_{42}<0.15$, while clusters from nearby hadronic showers are suppressed by requiring that candidates be at least 9° from all charged tracks.

Most photons satisfying these requirements are produced in π^0 decay. We reject a candidate that, when combined with any other photon, produces a mass between 0.117 GeV/c^2 and 0.147 GeV/c^2. The second photon must have energy greater than 30 MeV and LAT<0.8, with no requirement on A_{42} or distance from charged tracks.

A systematic error due to the photon selection criteria is obtained by comparing the branching ratio $\tau^+ \to h^+\pi^0\pi^0/\tau^+\to h^+\pi^0$ in data to that in simulation, where h^+ is any charged track. We also vary the minimum energy requirement from 0.10 to 0.14 GeV and test alternative π^0 veto regions. We obtain a systematic error of 3.1% for the χ_{c1} and 4.4% for the χ_{c2} common to both the e^+e^- and $\mu^+\mu^-$ final states. An additional component to the systematic error arises from changes in the shape of the background, shown in Fig. 3, affecting the fit results. It is specific to each final state and mode, and amounts to 2.2% (e^+e^-) and 1.3% ($\mu^+\mu^-$) for the χ_{c1}, and 9.2% (e^+e^-) and 11.9% ($\mu^+\mu^-$) for the χ_{c2}.

The photon is constrained to originate at the J/ψ vertex in the calculation of the χ_c four-momentum. We require p^* <1.7 GeV/c, a requirement that is satisfied by χ_{c1} or χ_{c2} mesons from B decays.

We determine the number of mesons from a fit to the plot of the mass difference between the candidate and the daughter J/ψ masses (Fig. 3). We use different signal pdfs for the χ_{c1} and χ_{c2}. These are formed by convolving the pdf calculated by simulation with a Gaussian distribution, where the offset and sigma are constrained to be the same for the χ_{c1} and χ_{c2}. The background is described by a third-order Chebychev polynomial. Systematic errors on the fit are obtained as for the J/ψ. The correlation coefficient between the number of χ_{c1} and χ_{c2} mesons obtained from the fit is 0.19.

Equation (4) is used to determine inclusive $B\to\chi_{c1}X$ and $B\to\chi_{c2}X$ branching fractions separately for $J/\psi\to e^+e^-$ and $J/\psi\to\mu^+\mu^-$. In this case, $\mathcal{B}_c=\mathcal{B}(\chi_{cJ}\to J/\psi\gamma)\cdot\mathcal{B}(J/\psi \to\ell^+\ell^-)$, where χ_{cJ} is χ_{c1} or χ_{c2} and ℓ is e or μ. Table I summarizes the yields, efficiencies, uncertainties and branching fraction products $\mathcal{B}(B\to\chi_{cJ}X)\cdot\mathcal{B}(\chi_{cJ}\to J/\psi\gamma)\cdot\mathcal{B}(J/\psi \to\ell^+\ell^-)$. The 4.5% ($\chi_{c1}$) and 5.3% ($\chi_{c2}$) systematic errors common to both e^+e^- and $\mu^+\mu^-$ include photon reconstruction in addition to the J/ψ reconstruction items.

As with the J/ψ, the inclusive B branching fractions to the χ_{c1} and χ_{c2} are calculated separately using the $J/\psi \to e^+e^-$ and $J/\psi\to\mu^+\mu^-$ decays. The two values are then combined, distinguishing uncertainties common to both from those unique to a single final state.

The branching fraction obtained for the χ_{c2} is comparable to that for the χ_{c1} and is summarized in Table II. This result is consistent with a prediction from a color octet calculation [16], and is in contrast to the expectation of a null result in a factorization calculation [17].

VII. $\psi(2S)$ PRODUCTION

The reconstruction of the $\psi(2S)$ in the $\ell^+\ell^-$ final state is very similar to the J/ψ reconstruction outlined in Sec. V A,

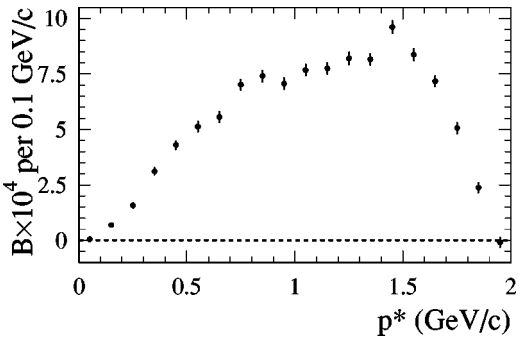

FIG. 6. $B \to J/\psi X$ branching fraction as a function of p^*.

with the p^* requirement tightened to $p^* < 1.6$ GeV/c. Figure 4 shows the resulting candidate mass distribution. A fit to extract the number of mesons in each plot is performed as for the J/ψ, but with the resolution and bremsstrahlung parameters fixed to the values found in the higher-statistics J/ψ channels. These parameters are varied according to their uncertainties as one contribution to the systematic error on the fit; the remaining contributions are determined as for the J/ψ.

These data are used to calculate the branching fraction product $\mathcal{B}(B \to \psi(2S)X) \cdot \mathcal{B}(\psi(2S) \to \ell^+\ell^-)$, and are later used in the determination of the p^* distribution of $\psi(2S)$ mesons produced in B decay. However, the extraction of the $B \to \psi(2S)X$ branching fraction requires the use of $\psi(2S) \to e^+e^-$ and $\psi(2S) \to \mu^+\mu^-$ branching fractions. Since this same data set has previously been used to measure these branching fractions [18], we do not use $\psi(2S) \to \ell^+\ell^-$ events to find $\mathcal{B}(B \to \psi(2S)X)$.

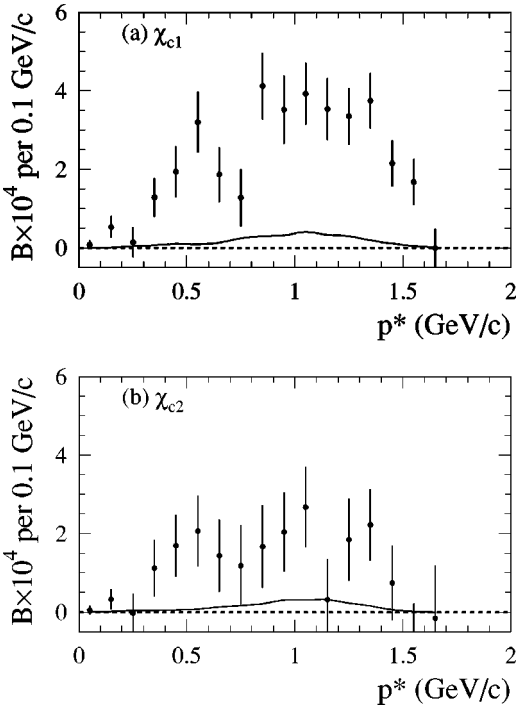

FIG. 7. Branching fraction as a function of p^* for (a) $B \to \chi_{c1}X$ and (b) $B \to \chi_{c2}X$. The distribution includes a small feed-down component from the $\psi(2S)$ (solid curve).

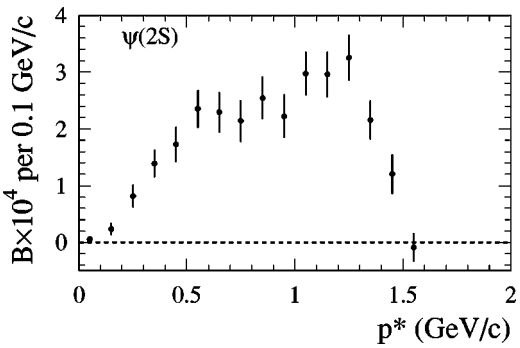

FIG. 8. $B \to \psi(2S)X$ branching fraction as a function of p^*.

Instead, we use $\psi(2S) \to J/\psi\pi^+\pi^-$ for this purpose. The reconstruction of a $\psi(2S)$ candidate in this final state starts with a J/ψ candidate satisfying the tighter mass constraints used in χ_{cJ} reconstruction. All charged particles, including those failing the ''good-track'' criteria, are assumed to be pion candidates. The pion pair is required to be oppositely charged and to have a mass, calculated by four-vector addition, in the range 0.45 to 0.60 GeV/c^2. The mass distribution from simulation is compared to the measured [19] distribution to obtain a systematic error of 0.5% on reconstruction efficiency. Finally, the p^* of the $\psi(2S)$ candidate is required to be less than 1.6 GeV/c.

Figure 5 displays the mass difference between the $\psi(2S)$ and the J/ψ candidates separately for $J/\psi \to e^+e^-$ and $J/\psi \to \mu^+\mu^-$. As for the other final states, the distributions are fit to obtain the number of mesons. The resolution smearing parameters are not required to be the same for the two plots, but are consistent: 1.5 ± 0.8 MeV/c^2 (e^+e^-) and 1.8 ± 0.5 MeV/c^2 ($\mu^+\mu^-$). The secondary branching fractions in Eq. (4) are in this case $\mathcal{B}_c = \mathcal{B}(\psi(2S) \to J/\psi\pi^+\pi^-) \cdot \mathcal{B}(J/\psi \to \ell^+\ell^-)$.

VIII. DIRECT BRANCHING FRACTIONS

To obtain the branching fraction for J/ψ mesons produced directly in the decay of B mesons, we subtract the feeddown contributions to the inclusive branching fraction due to the decay of χ_{c1}, χ_{c2}, and $\psi(2S)$ mesons. For the χ_{c1} and

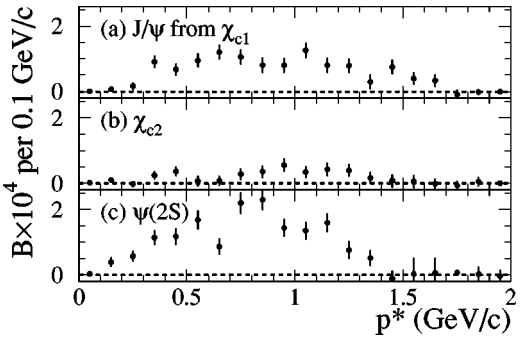

FIG. 9. Contributions to the $B \to J/\psi X$ branching fraction as a function of p^* due to feed-down from (a) χ_{c1}, (b) χ_{c2} and (c) $\psi(2S)$ mesons.

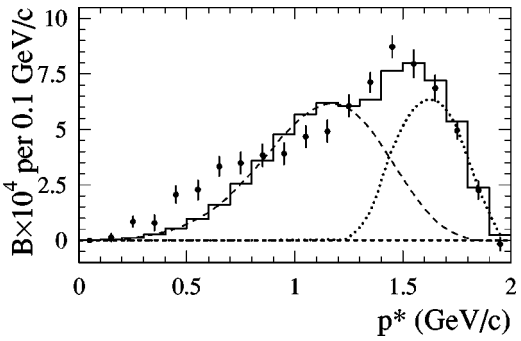

FIG. 10. p^* of J/ψ mesons produced directly in B decays (points). The histogram is the sum of the color-octet component from a recent NRQCD calculation [20] (dashed line) and the color-singlet $J/\psi K(*)$ component from simulation (dotted line).

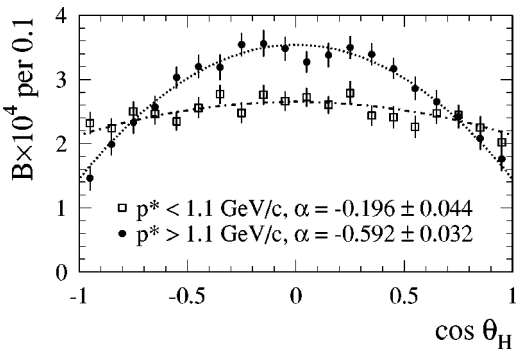

FIG. 11. Helicity of J/ψ mesons produced in B decay with $p^* > 1.1$ GeV/c (dots) and $p^* < 1.1$ GeV/c (open squares).

χ_{c2}, the feeddown branching fraction is $\mathcal{B}(B \to \chi_{cJ}X) \cdot \mathcal{B}(\chi_{cJ} \to J/\psi\gamma)$, while for the $\psi(2S)$, it is $\mathcal{B}(B \to \psi(2S)X) \cdot \mathcal{B}(\psi(2S) \to J/\psi X)$.

Similarly, the feeddown from the $\psi(2S)$ to the χ_{c1} and χ_{c2} is $\mathcal{B}(B \to \psi(2S)X) \cdot \mathcal{B}(\psi(2S) \to \chi_{cJ}\gamma)$.

Note that a number of uncertainties are common to both the inclusive and feeddown components, including track quality and particle identification criteria, $\mathcal{B}(\chi_{c1} \to J/\psi\gamma)$, and $\mathcal{B}(\chi_{c2} \to J/\psi\gamma)$. We use world average values [15] for the $\psi(2S)$ branching fractions. The resulting direct branching fractions are summarized in Table II.

IX. p^* DISTRIBUTIONS

The momentum distributions of charmonium mesons provide an insight into their production mechanisms. Since we do not fully reconstruct the B meson, we cannot determine the meson momentum in the B rest frame and instead use p^*, the value in the $\Upsilon(4S)$ center-of-mass frame. The difference, due to the motion of the B in the center-of-mass frame, has an rms spread of 0.12 GeV/c.

A. Inclusive p^* distributions

To measure the p^* distributions of J/ψ, χ_{c1}, χ_{c2}, and $\psi(2S)$ mesons produced in B decays, we create mass or mass-difference histograms of on-resonance candidates with p^* in the desired range. The e^+e^- and $\mu^+\mu^-$ final states are again treated separately. The distributions are then fit, with all signal pdf parameters (other than the number of mesons) fixed to the values obtained from the earlier fits. The fits are performed for 100 MeV/c wide p^* ranges, and in each case the sum of the yields differs from the original fit by fewer than ten events.

In the case of the J/ψ, we perform similar fits on the off-resonance data and perform a continuum subtraction for each p^* bin. Since there are no statistically significant off-resonance χ_{c1}, χ_{c2}, or $\psi(2S)$ signals, we do not perform a continuum subtraction in these cases.

The yield in each bin is corrected by the reconstruction efficiency obtained from simulated data, which decreases by approximately 10% between 0 and 2 GeV/c. The yield is then multiplied by an overall normalization factor for that particular final state and mode, which adjusts the sum of all bins to the earlier branching fraction measurement. We then perform a weighted average of the two distributions for the J/ψ, χ_{c1}, or χ_{c2}, or the four distributions for the $\psi(2S)$, to obtain the distributions shown in Figs. 6–8. For this purpose, we use the $\psi(2S) \to e^+e^-$ and $\psi(2S) \to \mu^+\mu^-$ branching fractions from Ref. [18]. In all cases, the distributions that are combined are consistent within statistical errors.

B. Direct p^* distributions

The J/ψ p^* distribution (Fig. 6) includes components due to mesons from the decays $\chi_{c1} \to J/\psi\gamma$, $\chi_{c2} \to J/\psi\gamma$, and $\psi(2S) \to J/\psi X$. To measure these distributions, we repeat the analysis with the data binned by the p^* of the J/ψ daughter. The resulting J/ψ feeddown distributions are presented in Fig. 9.

Note that we are using only the $J/\psi\pi^+\pi^-$ decay mode to obtain the J/ψ distribution from $\psi(2S)$ decay. In fact, 10.5% of $\psi(2S) \to J/\psi X$ decays are modes other than $J/\psi\pi\pi$. If we instead use the simulated J/ψ distribution for this 10.5%, Fig. 9c changes by no more than a small fraction of the statistical error bar in any bin.

Subtracting these three components from the inclusive J/ψ distribution in Fig. 6 leaves the contribution due to the J/ψ mesons produced directly in B decay (Fig. 10).

The superimposed histogram is a calculation of the expected distribution, which includes color octet and color singlet components. We use a recent NRQCD calculation [20] for the color octet component. The authors attribute the singlet component to $J/\psi K^{(*)}$ production, which we obtain from simulation. The two are normalized to obtain the best fit to our data. Possible sources of the apparent excess at low momentum are an intrinsic charm component of the B [21], the production, together with the J/ψ, of baryons [22], or an $s\bar{d}g$ hybrid [23].

The small feeddown contribution to χ_{c1} and χ_{c2} from $\psi(2S)$ decay is calculated by simulation and is shown in Fig. 7.

X. J/ψ HELICITY

The helicity θ_H of a $J/\psi \to \ell^+\ell^-$ candidate is the angle, measured in the J/ψ rest frame, between the positively

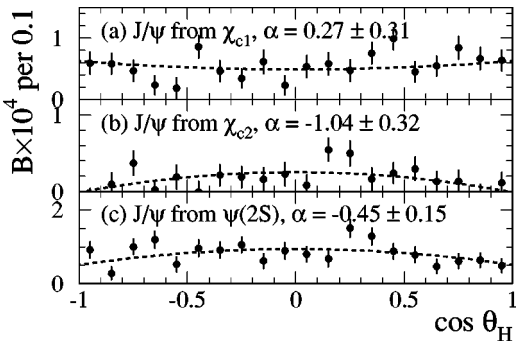

FIG. 12. Helicity distribution of J/ψ mesons produced in the decay of (a) χ_{c1}, (b) χ_{c2}, and (c) $\psi(2S)$ mesons.

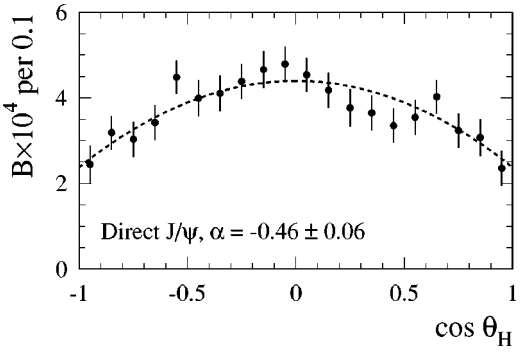

FIG. 13. Helicity distribution of J/ψ mesons produced directly in the decay of B mesons.

charged lepton and the flight direction of the J/ψ in the $\Upsilon(4S)$ center-of-mass frame. A more natural definition would use the B rest frame, but it cannot be determined in this analysis. Simulation indicates that the rms spread of the difference between the two definitions is 0.085 in $\cos\theta_H$.

A. Inclusive helicity distribution

We proceed as for the J/ψ p^* distribution, with data categorized into ranges of width 0.1 in $\cos\theta_H$ for two different momentum ranges, which we choose as $p^*<1.1$ GeV/c and $1.1<p^*<2.0$ GeV/c. We fit the on- and off-resonance mass distributions to obtain yields in each bin and perform a continuum subtraction. We correct using the reconstruction efficiency obtained from simulation for that range, although we observe little dependence of efficiency on helicity. We then apply separate normalization factors to the e^+e^- and $\mu^+\mu^-$ data such that the total branching fraction (summed over the two p^* ranges) agrees with the value obtained earlier for that mode. The distributions from e^+e^- and $\mu^+\mu^-$ are consistent and are averaged to obtain the helicity distributions for each of the two p^* ranges (Fig. 11).

We fit each distribution with a function $1+\alpha\cdot\cos^2\theta_H$ to obtain the polarization α, where $\alpha=0$ indicates the sample is unpolarized, $\alpha=1$ transversely polarized, and $\alpha=-1$ longitudinally polarized. The high p^* region, which includes the two-body B decays, is more highly polarized, $\alpha=-0.592\pm0.032$, than the lower p^* region, $\alpha=-0.196\pm0.044$.

We assign a systematic error of 0.008 to these polarizations by instead considering the reconstruction efficiency to be independent of helicity.

B. Direct J/ψ helicity

We determine the helicity distributions of J/ψ mesons produced in the decay of χ_{c1}, χ_{c2}, and $\psi(2S)$ in the same way we calculate the p^* feeddown. Because of the limited statistics of these samples, we combine the two momentum regions used in the inclusive analysis. The resulting feeddown helicity distributions are shown together with the polarization fits in Fig. 12. We subtract these from the sum of the two distributions in Fig. 11 to obtain the helicity distribution for the J/ψ produced directly in B decay (Fig. 13). The polarization, $\alpha=-0.46\pm0.06$, is slightly out of the range -0.33 to 0.05 predicted by an NRQCD calculation [24], but other authors have argued [25] that relativistic corrections reduce the reliability of the calculation. The systematic uncertainty of 0.008 obtained above is small compared to the statistical error. This result is difficult to compare directly with that from Collider Detector at Fermilab (CDF) [26], due to the different mixture of b mesons and baryons, and the distinction between the effective helicity calculated there and the true helicity.

XI. SUMMARY

We have reported new measurements of B meson decays to final states including charmonium mesons, which are summarized in Table II. We have presented a number of momentum distributions. The distributions of the feeddown J/ψ daughters of the χ_{c1}, χ_{c2}, and $\psi(2S)$ have not previously been measured, and allow us to more accurately determine the distribution for J/ψ mesons produced directly in B decay. The direct J/ψ distribution is compared to a recent NRQCD calculation and appears to indicate an excess at low momentum.

The J/ψ helicity distribution, which has also has not previously been published, indicates that the polarization of direct J/ψ mesons is slightly out of the range predicted by an NRQCD calculation.

ACKNOWLEDGMENTS

We are grateful for the excellent luminosity and machine conditions provided by our PEP-II colleagues, and for the substantial dedicated effort from the computing organizations that support *BABAR*. The collaborating institutions wish to thank SLAC for its support and kind hospitality. This work is supported by DOE and NSF (USA), NSERC (Canada), IHEP (China), CEA and CNRS-IN2P3 (France), BMBF (Germany), INFN (Italy), NFR (Norway), MIST (Russia), and PPARC (United Kingdom). Individuals have received support from the A. P. Sloan Foundation, Research Corporation, and Alexander von Humboldt Foundation.

[1] G. T. Bodwin, E. Braaten, and G. P. Lepage, Phys. Rev. D **51**, 1125 (1995); **55**, 5853(E) (1997); M. Beneke, F. Maltoni, and I. Z. Rothstein, *ibid.* **59**, 054003 (1999).
[2] E. Braaten and S. Fleming, Phys. Rev. Lett. **74**, 3327 (1995); M. Cacciari, M. Greco, M. L. Mangano, and A. Petrelli, Phys. Lett. B **356**, 553 (1995).
[3] CDF Collaboration, F. Abe *et al.*, Phys. Rev. Lett. **69**, 3704 (1992); **79**, 572 (1997); **79**, 578 (1997); D0 Collaboration, S. Abachi *et al.*, Phys. Lett. B **370**, 239 (1996).
[4] A. K. Leibovich, Nucl. Phys. B (Proc. Suppl.) **93**, 182 (2001); G. A. Schuler, Eur. Phys. J. C **8**, 273 (1999).
[5] CLEO Collaboration, R. Balest *et al.*, Phys. Rev. D **52**, 2661 (1995); S. Chen, *et al.*, *ibid.* **63**, 031102 (2001).
[6] Belle Collaboration, K. Abe *et al.*, Phys. Rev. Lett. **89**, 011803 (2002).
[7] *BABAR* Collaboration, B. Aubert *et al.*, Nucl. Instrum. Methods Phys. Res. A **479**, 1 (2002).
[8] ''GEANT Detector Description and Simulation Tool,'' Version 3.21, CERN Program Library Long Writeup W5013, 1994.
[9] G. C. Fox and S. Wolfram, Phys. Rev. Lett. **41**, 1581 (1978).
[10] T. Sjostrand, Comput. Phys. Commun. **82**, 74 (1994).
[11] A. Drescher *et al.*, Nucl. Instrum. Methods Phys. Res. A **237**, 464 (1985). LAT$=\Sigma_{i=3}^{n}E_i r_i^2/(E_1 r_0^2+E_2 r_0^2+\Sigma_{i=3}^{n}E_i r_i^2)$, where the *n* crystals in the EMC cluster are ranked in order of energy deposited in that crystal, E_i, and $r_0=5$ cm is the average distance between crystal centers. r_i is the distance between crystal *i* and the cluster centroid calculated from an energy-weighted average of the *n* crystals.
[12] R. Sinkus and T. Voss, Nucl. Instrum. Methods Phys. Res. A **391**, 360 (1997). The Zernike moment A_{nm} is calculated using the energy E_i and location (ρ_i,ϕ_i) of crystals with respect to the shower centroid. The location is defined in a cylindrical coordinate system with the *z* axis running from the beam spot to the centroid, where $\rho_i=r_i/R_0$ and $R_0=15$ cm. $A_{nm}=\Sigma_{i=1}^{n}(E_i/E)\cdot f_{nm}(\rho_i)e^{-im\phi_i}$, where the sum includes only crystals with $\rho_i\leqslant 1$, and E is the total energy in the cluster. The Zernike functions are $f_{nm}(\rho)=\Sigma_{s=0}^{(n-m)/2}[(-1)^s(n-s)!\rho^{n-2n}/s!((n+m)/2-s)!((n-m)/2-s)!]$, with $m\leqslant n$ and $(n-m)$ even. Studies indicate that A_{42} provides good separation between hadronic and electromagnetic showers when used in conjunction with LAT.
[13] *BABAR* Collaboration, B. Aubert *et al.*, Phys. Rev. Lett. **87**, 162002 (2001); Belle Collaboration, K. Abe *et al.*, *ibid.* **88**, 052001 (2002).
[14] E. Barberio, B. van Eijk, and Z. Was, Comput. Phys. Commun. **66**, 115 (1991).
[15] Particle Data Group, K. Hagiwara *et al.*, Phys. Rev. D **66**, 010001 (2002).
[16] G. T. Bodwin, E. Braaten, T. C. Yuan, and G. P. Lepage, Phys. Rev. D **46**, 3703 (1992).
[17] J. H. Kühn, S. Nussinov, and R. Rückl, Z. Phys. C **5**, 117 (1980).
[18] *BABAR* Collaboration, B. Aubert *et al.*, Phys. Rev. D **65**, 031101 (2002).
[19] BES Collaboration, J. Z. Bai *et al.*, Phys. Rev. D **62**, 032002 (2000).
[20] M. Beneke, G. A. Schuler, and S. Wolf, Phys. Rev. D **62**, 034004 (2000). Curve is from Fig. 5, $\Lambda=300$ MeV, $p_F=300$ GeV, and $m_{sp}=150$ MeV.
[21] C.-H. V. Chang and W.-S. Hou, Phys. Rev. D **64**, 071501 (2001).
[22] S. J. Brodsky and F. S. Navarra, Phys. Lett. B **411**, 152 (1997).
[23] G. Eilam, M. Ladisa, and Y.-D. Yang, Phys. Rev. D **65**, 037504 (2002).
[24] S. Fleming *et al.*, Phys. Rev. D **55**, 4098 (1997).
[25] J. P. Ma, Phys. Rev. D **62**, 054012 (2000).
[26] CDF Collaboration, T. Affolder *et al.*, Phys. Rev. Lett. **85**, 2886 (2000).